Mathematical Models and Methods in Applied Sciences

Vol. 0, No.0 (2001) 000–000

SIMULATION OF SOME QUANTUM MODELS FOR SEMICONDUCTORS*

Ph. CAUSSIGNAC†, J. DESCLOUX‡and A. YAMNAHAKKI §
Département de Mathématiques,
Ecole Polytechnique Fédérale de Lausanne,
CH-1015 Lausanne, Suisse

(Leave 1 inch blank space for publisher.)

Three different existing steady-state models with quantum correction for simulating the resonant tunnelling diode are summarized. Numerical methods are briefly described and also a theoretical argument for one of the models. Results of simulation are focused on the capability of reproducing the negative differential resistivity.

1. Introduction

The goal of this paper is to simulate some models for semiconductor devices incorporating quantum effects in order to check their ability to reproduce quantum phenomena. The main physical property we are interested in is the so-called negative differential resistivity of the resonant tunneling diode (**RTD**)[23]: the current versus voltage (**IV**) curves have local maxima and consequently regions where the current decreases for increasing voltage.

The choice of the RTD device is principally motivated by its one-dimensional computational domain and also its "pure" quantum behaviour, that is the IV curve can be explained only by some term stemming from quantum mechanics. Nethertheless, **RTD**'s have a large area of physical applications, such as high-frequency signal generation, high-speed switching and multi-valued data storage.

During the last years, an increasing effort has been done in developing and analysing models capable of reproducing quantum phenomena.The Schroedinger-Poisson (**SP**) system has been widely used to describe the quantum-mechanical wave-nature of electrons (see for instance [24], [7],[25], [18] for the equilibrium steady state). Under applied voltage, the tunnelling properties of the semiconductor structure can also be simply reproduced by using the transmission probability function, which is obtained by solving the current carrying SP models with absorbing boundary conditions, see [5], [3], [1], [11]. A proper theoretical description of the complicated

*This work has been partly supported by the Swiss National Science Foundation under grant no. 20-40425.94
†E-mail: philippe.caussignac@epfl.ch
‡E-mail: jean.descloux@epfl.ch
§E-mail: ayamnahakki@vaudoise.ch

transport properties is given in terms of the Heisenberg equation for the density matrix, or equivalently of the kinetic-like quantum-Liouville equation for the Wigner function, with additional terms representing collisional processes. Both the density matrix and Wigner function, have been solved numerically in order to analyze electron quantum transport in RTD's, see [10], [21], [17].

At low level of accuracy in the hierarchy of these quantum models, the Quantum HydroDynamical (**QHD**) models[12], [13] or the Quantum Drift-Diffusion (**QDD**) models [3], [27], [30] have begun to attract the attention of applied mathematicians, because of their capability to give a correct macroscopic description of the quantum properties of the semiconductor structures at a reasonable cost, and to avoid some implementation related to the other quantum models. Various versions of QHD and QDD models appeared in the literature depending on the way of derivation and/or on the closure conditions. For example, the zero quantum space charge model, a model simpler than the QDD one for an isothermal quantum fluid, is presented and rigourously derived as an asymptotic limit in[29].

In **Section 2**, we describe in some details the RTD and specify its geometry. While the geometry of the device itself (the two barriers and the well) are fixed, the length of the computational domain can be changed for a good matching of the boundary conditions. We next present our three basic kinds of models:

1. The standard QHD and QDD models (derived assuming that the potential energy is a smooth function, the QDD model being a particular case of the QHD model without the energy equation nor the convection term in the momentum equation)

2. The smooth QHD and QDD models which are derived for discontinuous potential

3. The Schroedinger-Poisson model.

The first two kinds of models are very like their classical form but include some correction terms of quantum nature.

The numerical methods used for simulating the standard QHD and QDD models are given in **Section 3,** and followed by numerical results. In our computations, we used two different devices (i.e. two sets of physical parameters) corresponding to those or References[12], [21]. The main reason for that was to compare and try to reproduce the results of these papers, because the models are quite sensitive to the physical parameters.

In **Section 4** (resp. **Section 5)**, we proceed likewise to present numerical methods and results for the smooth QDD models and the Schoedinger-Poisson model respectively. Furthermore, **Section 4** contains a paragraph for an argument showing that the smooth QDD model is not tractable when the potential barriers are too high. A short conclusion is given in **Section 6**.

2. The device and the models

2.1. *The resonant tunnelling diode*

A resonant tunnelling diode (Fig. 1) typically consists of an undoped quantum well layer sandwiched between undoped barrier layers and heavily doped emitter and collector contact regions , see [23] and references therein . The most common double barrier system is based on the $Al_xGa_{1-x}As$(barrier)/GaAs(well)/$Al_xGa_{1-x}As$ (Barrier) heterostructure.

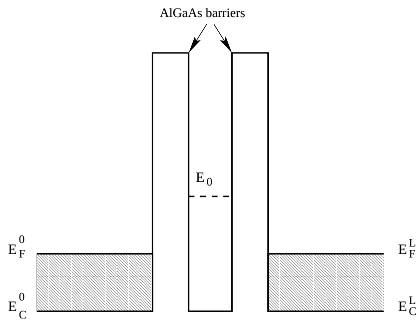

Fig. 1a. Equillibrium state

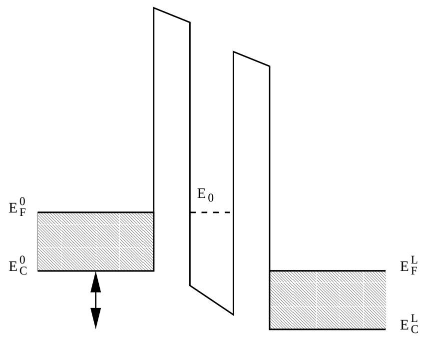

Fig. 1b. Threshold state

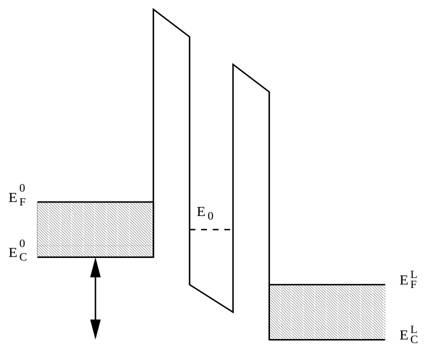

Fig. 1c. Resonant state

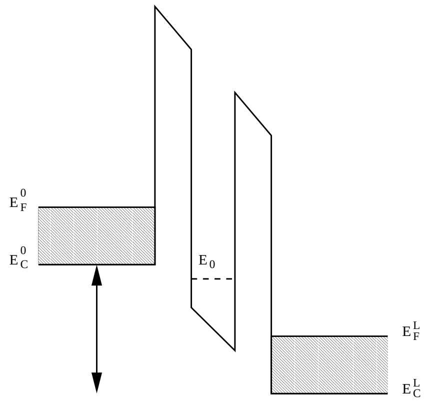

Fig. 1d. Off-resonant state

The RTD is thus an open quantum system in which the electronic states are scattering states with a continuous distribution in energy space, rather than bounded states with a discrete energy spectrum. Under these circumstances quasi-bounded states (resonant states) are formed in the quantum well which accommodate electrons for a time that is a characteristic of the double-barrier structure (the lowest state is denoted E_0 in the diagram).
The conduction-band diagrams for the RTD under four bias conditions are shown in Fig.1(a)-(d): (a) at zero bias, (b) at threshold, (c) at resonance and (d) at off-

resonance. The so-called 'resonant' tunnelling through the double barrier structure occurs when the energy of the electrons flowing from the emitter coincides with the energy of the quasi-bounded state E_0, in the quantum well. The effect of the external bias V is to sweep the alignment of the emitter and quasi-bounded states. Thus a resonant tunnelling current starts to flow when E_0 reaches the quasi-Fermi level E_F^0, in the emitter (Fig. 1(b): the threshold state of the RTD), reaches its maximum when E_0 passes through the Fermi sea in the emitter (Fig. 1(c):the resonant state) and stops to flow when E_0 falls below the conduction band edge in the emitter(Fig. 1(d):the off-resonant state).

The geometry of the device that we want to simulate is the following one. The width of both barriers and the well are equal to 50Å; the right boundary is placed at the origin and the left boundary at L. This total length can vary from 200Å to 500Å in order to match correctly the boundary conditions, keeping the entire device symmetric.

2.2. *Quantum drift-diffusion and hydrodynamic models*

The simplest fluid model including quantum effects consists in writing the single state solution of the Schroedinger equation in the modulus-phase representation used for the WKB method. We then get the so-called Madelung fluid equations of quantum mechanics, involving the electron current and density, the correction term to the classical Euler equations being the Bohm potential [22],[16] of order $\hbar^2$. Of course, this model has no temperature because it represents a single (pure) state.

In the further step, one considers the quantum mechanics of a mixed state; Gasser et al.[16] used the same type of WKB representation for all single states of a mixed state and obtained equations for the density, current and energy tensor which lead straightforwardly to the standard quantum hydrodynamic model (without collisions). The only term which has to be closed in these equations is the heat flux tensor, which will usually be modelized by the classical Fourier law. The nonlinear collision terms are added by hand and chosen to be given by a relaxation term. To our mind this derivation of the hydrodynamic quantum model is the easiest and simplest one.

For a 3D geometry, the equations of the quantum hydrodynamic model read:

$$\frac{\partial n}{\partial t} + div(n\mathbf{u}) = 0, \tag{2.1}$$

$$\frac{\partial}{\partial t}(nm\mathbf{u}) + div(mn\mathbf{u} \otimes \mathbf{u} - \mathbf{P}) + n\nabla V = -\frac{1}{\tau_p}(mn\mathbf{u}), \tag{2.2}$$

$$\frac{\partial W}{\partial t} + div(\mathbf{u}W - \mathbf{u}\cdot\mathbf{P} - \varkappa\nabla T) + n\mathbf{u}\cdot\nabla V = -\frac{(W - \frac{3}{2}n\ \mathrm{k}_B T_0)}{\tau_w}, \tag{2.3}$$

$$-div(\varepsilon \nabla \phi) = \frac{q}{\varepsilon_0}(N_D - n), \tag{2.4}$$

with the potential energy

$$V = -(q\phi + \chi), \tag{2.5}$$

the stress tensor

$$\mathbf{P} = -n\mathrm{k}_B T\mathbf{I} + \frac{\hbar^2 n}{4m}\nabla \otimes \nabla \ln(n) \tag{2.6}$$

and the total energy

$$W = \frac{3}{2}n\mathrm{k}_B T + \frac{1}{2}mn\left|\mathbf{u}\right|^2 - \frac{\hbar^2 n}{8m}\triangle \ln(n). \tag{2.7}$$

The unknowns are the electronic density n, the particles velocity $\mathbf{u}$, the temperature T and the electrostatic potential ϕ. The material dependent quantities are the relaxation times τ_p and τ_w , the heat conductivity κ, the dielectric permittivity ε and the electronic affinity χ . The constants ε_0, k_B and $q > 0$ represent respectively the vacuum permittivity, the elementary charge and the Boltzmann constant, while the function N_D stands for the doping profile. We assume troughout this paper that the effective mass m of the electrons is constant.

Another method for deriving such equations for the QHD model consists in using the moments of the Wigner equation to get a hydrodynamic model with quantum corrections. First, let us notice that if we want to get quantum corrections to the classical hydrodynamic model from the Wigner equation, these can be obtained only by closure of the stress tensor or the heat flux terms since the first three moments yield the same equations as the moments of the Boltzmann equation. The general idea for closing the stress tensor is to compute this quantity using an approximation of the solution of the Wigner equation, e.g. the equilibrium solution or an approximation of it. This kind of method has been initiated by Gardner[12]; using the Hilbert expansion for the equilibrium solution of the Wigner equation [31], one computes the resulting stress-tensor and writes it in term of the macroscopic equilibrium quantities, and then replaces the latters by the unknowns. In this model, the heat flux has to be added by hand and, as in the preceeding case, it is closed with the Fourier law. Curiously enough, the quantum correction terms (of order $\hbar^2$) of this model is three times smaller than those in eqns (2.6) and (2.7). Furthermore, the equations are derived by assuming that the potential is twice differentiable, which is certainly not true for the resonant tunnelling diode. The model presented in the next section can be established without this regularity assumption.

Another and easier way to get QHD equations from the equilibrium Wigner distribution is to consider, in the case of Boltzmann statistics, the so-called Bloch equation satisfied by the density "matrix" [28]. From this equation, one can, for a regular potential, deduce an asymptotic expansion in $\hbar^2$ for the equilibrium Wigner function; keeping the first two terms yields the model of Gardner[12].

In this paper, we will consider the particular case of steady-state models applied to the one-dimensional RTD; this means that the unknowns depend only on one space coordinate, say x, varying in the interval $[0, L]$. Denoting by f' the derivative of a function f, we can write the equations for the unknowns $(\phi, J = nu, n, T)$ of the QHD model in this particular case:

$$-(\varepsilon\phi')' = \frac{q}{\varepsilon_0}(N_D - n) \text{ in } (0, L), \tag{2.8}$$

$$J' = 0 \text{ in } (0, L), \tag{2.9}$$

$$m\left(\frac{J^2}{n}\right)' + k_B\,(nT)' - \frac{\hbar^2}{4m}\,(n(\ln n)'')' + nV' = -\frac{m}{\tau_p}J \text{ in } (0, L), \tag{2.10}$$

$$\frac{5}{2}Jk_BT' + \frac{mJ^3}{2}(\frac{1}{n^2})' - \frac{3\hbar^2}{8m}J\,((\ln n)'')' - (\kappa T')' + JV' =$$

$$-\frac{1}{\tau_w}(\frac{3}{2}k_Bn(T - T_o) + \frac{mJ^2}{2n} - \frac{\hbar^2 n}{8m}(\ln n)'') \text{ in } (0, L). \tag{2.11}$$

Notice that here J is the particle current and not the electric current $-qnu$.

Like the QHD model, the quantum drift-diffusion (QDD) model can also be obtained by closure of the momenta of the Wigner equation, but in the small temperature limit[15]. The existence of solutions of the QDD model has been proved [4], its equations being characterized as the Lagrange equations of an energy functional. The QDD model consists only in equations (2.8), (2.9) and

$$k_BT_0n' - \frac{\hbar^2}{4m}\,(n(\ln n)'')' + nV' = -\frac{m}{\tau_p}J \text{ in } (0, L), \tag{2.12}$$

in place of (2.10); in Equ. (2.12), T_0 is the constant (lattice) temperature. We will call the model made of equations (2.8), (2.9) and (2.10), the isothermal QHD model.

Appropriate boundary conditions will be given later for the specific example of the RTD.

2.3. *The smooth QDD and QHD models*

These models are derived using an approximation of the equilibrium Wigner equation to compute the stress tensor and the energy as described in the preceeding paragraph. Since we will need them below, we first recall some equations. The quantum density matrix $\widetilde{\rho}$ is related to the Wigner distribution w by:

$$\widetilde{\rho}(\mathbf{R},\mathbf{s};\beta) = \int_{\Re^3} w(\mathbf{R},\mathbf{p};\beta)\exp(\frac{i}{\hbar}\mathbf{s}\cdot\mathbf{p})\ d\mathbf{p}, \tag{2.13}$$

with the center-of-mass coordinates:

$$\mathbf{R} = \frac{\mathbf{x}+\mathbf{y}}{2},\ \ \mathbf{s} = \mathbf{x}-\mathbf{y}, \tag{2.14}$$

and the explicit temperature dependence through $\beta = 1/k_BT$. The moments of the Wigner distribution are easily computed using

$$\langle \mathbf{p}^\alpha \rangle = \int_{\Re^3} w(\mathbf{x},\mathbf{p};\beta)\ \mathbf{p}^\alpha\ d\mathbf{p} = \left(\frac{\hbar}{i}\right)^{|\alpha|} \left(D_s^\alpha \widetilde{\rho}(\mathbf{R},\mathbf{s};\beta)\right)_{\mathbf{s}=\mathbf{0}}, \tag{2.15}$$

where α denotes a multi-index.

At equilibrium the density matrix $\rho_e(\mathbf{x},\mathbf{y};\beta) = \widetilde{\rho}_e(\frac{\mathbf{x}+\mathbf{y}}{2},\mathbf{x}-\mathbf{y};\beta)$ in the case of Boltzmann statistics is solution of the Bloch equation:

$$\frac{\partial \rho_e}{\partial \beta}(\mathbf{x},\mathbf{y};\beta) = \frac{\hbar^2}{2m}\triangle_{\mathbf{x}}\rho_e(\mathbf{x},\mathbf{y};\beta) - V(\mathbf{x})\rho_e(\mathbf{x},\mathbf{y};\beta),\ \ \mathbf{x},\mathbf{y}\in\Re^3,\ \ \beta>0, \tag{2.16}$$

with the initial condition

$$\rho_e(\mathbf{x},\mathbf{y};0) = \delta(\mathbf{x}-\mathbf{y}). \tag{2.17}$$

In the smooth models[13], the approximate density matrix is given in function of the equilibrium one by:

$$\widetilde{\rho}(\mathbf{R},\mathbf{s};\beta) \approx n(R)\frac{\widetilde{\rho}_e(\mathbf{R},\mathbf{s};\beta)}{\widetilde{\rho}_e(\mathbf{R},\mathbf{0};\beta)}e^{i\frac{m}{\hbar}\mathbf{s}\cdot\mathbf{u}}; \tag{2.18}$$

the normalization factor $1/\widetilde{\rho}_e(\mathbf{R},\mathbf{0};\beta)$ is introduced for having $n(\mathbf{x}) = \widetilde{\rho}(\mathbf{x},\mathbf{0};\beta)$ and the exponential corresponds to a shifted density matrix

$$w(\mathbf{R},\mathbf{p};\beta) = \frac{n(R)}{\widetilde{\rho}_e(\mathbf{R},\mathbf{0};\beta)}w_e(\mathbf{R},\mathbf{p}-m\mathbf{u};\beta),$$

with

$$\widetilde{\rho}_e(\mathbf{R},\mathbf{0};\beta) = \int_{\Re^3} w_e(\mathbf{R},\mathbf{p};\beta)\exp(\frac{i}{\hbar}\mathbf{s}\cdot\mathbf{p})\ d\mathbf{p}.$$

This shifted density matrix is usually used to establish the equations of the hydrodynamic model within the moment method.

Instead of using the true equilibrium density matrix in (2.18), this one will be further approximated. With the help of the Green function of the heat equation, eqs (2.16-2.17) yield an integral equation for the equilibirum Wigner function; the solution of this equation is replaced by the first two terms of the Neumann expansion, which constitutes the so-called Born approximation. A few other minor simplifications allow to compute an explicit approximate form of the Wigner function, which depends on integrals of a function of the potential; finally, by computing the moments, one obtains equations depending on the smoothed potential:

$$\overline{V}(\mathbf{x};\beta) = \int_0^1 d\beta'\beta'^2 \int_{\Re^3} \frac{d\mathbf{x}'}{\pi^{3/2}} \exp(-\mathbf{x}'^2) V(\mathbf{x} + \sqrt{\frac{\beta(1-\beta'^2)}{2m}}\mathbf{x}'). \tag{2.19}$$

The stress tensor and total energy for the smooth QHD model are given by

$$\mathbf{P} = -n\mathrm{k}_B T\mathbf{I} - \frac{\hbar^2 n}{4mT}\nabla \otimes \nabla\overline{V}, \tag{2.20}$$

$$W = \frac{3}{2}n\mathrm{k}_B T + \frac{1}{2}mn\left|\mathbf{u}\right|^2 + \frac{\hbar^2 n}{8mT}\triangle\overline{V}. \tag{2.21}$$

The full set of equations for the steady state problems in one dimension is the following one:

$$-(\varepsilon\phi')' = \frac{q}{\varepsilon_0}(N_D - n) \text{ in } (0,L), \tag{2.22}$$

$$J' = 0 \text{ in } (0,L), \tag{2.23}$$

$$m\left(\frac{J^2}{n}\right)' + k_B\,(nT)' + \frac{\hbar^2}{4m}\left(\frac{n}{T}\overline{V}''\right)' + nV' = -\frac{m}{\tau_p}J \text{ in } (0,L), \tag{2.24}$$

$$\frac{5}{2}Jk_BT' + \frac{mJ^3}{2}(\frac{1}{n^2})' - \frac{3\hbar^2}{8m}J\left(\frac{\overline{V}''}{T}\right)' - (\kappa T')' + JV' =$$

$$-\frac{1}{\tau_w}(\frac{3}{2}k_Bn(T-T_o) + \frac{1}{2n}mJ^2 + \frac{\hbar^2 n}{8mT}\overline{V}'') \text{ in } (0,L). \tag{2.25}$$

According to its authors, this model is valid for $\beta(\max V - \min V\ )$ small, which is certainly not the case for a RTD at low temperature.

Again, the analogous drift-diffusion model is obtained by dropping (2.25), replacing T by the constant lattice temperature T_0 and canceling the term containing J^2 in (2.24).

Recently, the QDD model has been derived using the operator form of the Wigner equation and the moment method for variable effective mass[30]; the integral for the smoothed potential has been worked out, resulting in a more practical form. But, the numerical results for a MOS diode and a MOSFET occured in the so-called slow varying potential approximation, which is the lower order of $\overline{V}$, which turns out to be equivalent to the QDD model of the preceeding section.

2.4. *The Schroedinger-Poisson model*

The basic idea for this model is to compute the current resulting from scattering states of the Schroedinger equation. This model is slightly different from the the preceeding ones since the collision effects obtained through the relaxation mechanism can not be included, at least to our knowledge. On the other side it has less physical parameters and may be easier to fit to experiments.

A very good summary of this kind of models can be found in [5]. The detailed form of the statistics density function is obtained from the Tsu-Esaki model presented in [23], chapter 2.

The scattering states are incident plane waves of momentum $\hbar k$ coming from $-\infty$ (Ψ_k^+) or $+\infty$ (Ψ_k^-). These states correspond to solutions of the one dimensional Schroedinger problems

$$-\frac{\hbar^2}{2m}\psi_k''(x) + V(x)\psi_k(x) = E\psi_k(x), \quad x \in (0, L), \tag{2.26}$$

$$(\psi_k^+)'(0) + ik_0\psi_k^+(0) = 2ik_0, \quad (\psi_k^+)'(L) - ik_L\psi_k^+(L) = 0, \tag{2.27}$$

$$(\psi_k^-)'(0) + ik_0\psi_k^-(0) = 0, \quad (\psi_k^-)'(L) - ik_L\psi_k^-(L) = -2ik_L e^{-ik_L L}. \tag{2.28}$$

In these equations, $E = \frac{\hbar^2 k^2}{2m}$ denotes the energy of the state ψ_k and we set $k_0 = +\sqrt{\frac{2m}{\hbar^2}(E - V_0)}$, $k_L = +\sqrt{\frac{2m}{\hbar^2}(E - V_L)}$, where $V_0 = V(0)$, $V_L = V(L)$ are the potential energies at the boundary of the computation domain.

At $\pm\infty$ the sources of the incident plane waves are mixed using Fermi-Dirac statistics; computing the current due to wave functions of the form $\psi_k(x)e^{ik_y y}e^{ik_z z}$ and integrating over the whole $k_y - k_z$-space yield finally a probability factor proportional to $\ln(1 + e^{\frac{\mu - E}{k_B T}})/\sqrt{E}$. The total electronic current is then obtained from the formula

$$J = \frac{qmkT_0}{2\pi^2\hbar^3}\int_{V_0}^{\infty} \ln\left(\frac{1 + \exp\frac{\mu_0 - E}{kT_0}}{1 + \exp\frac{\mu_L - E}{kT_0}}\right) T(E)dE, \tag{2.29}$$

where the transmission probability is given by

$$T(E) = \frac{k_L}{k_0}\left|\psi_k^+(L)\right|^2 = \frac{k_0}{k_L}\left|\psi_k^-(0)\right|^2, \ \mathrm{E{>}V_0}, \tag{2.30}$$

and μ_0 (resp. μ_L) are the local Fermi energies at the left (resp. the right) extremity of the domain.

The **L**inearized **S**chroedinger-**P**oisson model **(LSP)** uses a given approximation of the electrostatic potential for computing J from eqns (2.26-2.30).

The true SP model is obtained from equations (2.26-2.30) together with a coupling of the Poisson equation (2.8) through the electronic density given by

$$\begin{aligned} n(x) = & \left(\frac{m}{\hbar}\right)^{3/2} \frac{\sqrt{2}k_B T_0}{4\pi^2} \times \\ & \left\{ \int_{V_0}^{\infty} \frac{1}{(E-V_0)^{1/2}} |\psi_k^+(x)|^2 \ln\left(1+\exp(\frac{\mu_0 - E}{k_B T_0})\right) dE \right. \\ & \left. + \int_{V_L}^{\infty} \frac{1}{(E-V_L)^{1/2}} |\psi_k^-(x)|^2 \ln\left(1+\exp(\frac{\mu_L - E}{k_B T_0})\right) dE \right\}. \end{aligned} \tag{2.31}$$

3. Results for the QDD and QHD models

3.1. *Numerical method*

Our goal is to get a formulation of the QHD (and of course also of the QDD) model which consists in a system of first order nonlinear differential equations with boundary conditions and depending on one continuation parameter, e.g. the applied drain-source voltage.

For the hydrodynamic model, we integrate (2.9) by setting J as an unknown constant into the other equations. The boundary conditions are then given by

$$\phi(0) = -V_{app}, \ \phi(1) = 0,$$

$$n(0) = n(L) = N_D(0), \ n'(0) = n'(L) = 0,$$

$$T(0) = T(L) = T_0,$$

with $-V_{app}$ the applied voltage and T_0 the lattice temperature.

By using the total length of the computation domain $L_0 = L$ and introducing the reference relaxation time τ_0 and furthermore, for scaling reasons, the reference doping profile $N_D^{max} = \underset{x\in[0,L]}{max} N_D(x)$ and heat coefficient κ_0, we rewrite eqs (2.10), (2.11) and (2.8), keeping the same notations for the dimensionless variables as

$$\left(\beta\frac{J^2}{n} + nT - \alpha n(\ln n)''\right)' - n(\phi+\chi)' = -\frac{J}{\tau_p} \text{ in } (0,1), \tag{3.32}$$

$$\left(\frac{J}{n}\left(\frac{5}{2}nT + \beta\frac{J^2}{2n} - \frac{3}{2}\alpha n(\ln n)''\right) - \gamma\kappa T' - J(\phi+\chi)\right)' =$$

$$-\frac{1}{2\beta\tau_w}(3kn(T-1)+\beta\frac{J^2}{n}-\alpha n(\ln n)'') \text{ in } (0,1), \tag{3.33}$$

$$-(\varepsilon\phi')' = \sigma(N_D - n) \text{ in } (0,1). \tag{3.34}$$

We have used the following constants:

$$\alpha = \frac{\hbar^2}{4mL_0^2 k_B T_0},\ \beta = \frac{k_B T_0 \tau_0^2}{mL_0^2},$$

$$\sigma = \frac{q^2 N_D^{max} L_0^2}{\varepsilon_0 k_B T_0},\ \gamma = \frac{m\kappa_0}{\tau_0 k_B^2 T_0 N_D^{max}};$$

notice that the energy quantities are in units of $k_B T_0$ and the current is scaled by

$$J_0 = \frac{k_B T_0 \tau_0 N_D^{max}}{mL_0}. \tag{3.35}$$

Before defining our first order system, we make the change of variable $u = \ln n$ in eqs (3.32-3.34); finally, we introduce the new unknowns:

$$y_1 = u,\ y_2 = u',\ y_3 = -\alpha u'' e^u + \beta J^2 e^{-u} + T - e^u(\phi+\chi), \tag{3.36}$$

$$y_4 = T,\ y_5 = \frac{5}{2}JT + \frac{\beta}{2}J^3 e^{-2u} - \frac{3\alpha}{2}Ju'' - J(\phi+\chi), \tag{3.37}$$

$$y_6 = \phi,\ y_7 = \varepsilon\phi'. \tag{3.38}$$

Notice that these new unknowns are continuous at the layer interfaces. Now, with the help of (3.32-3.34) and the definitions (3.36-3.38), we get our final system:

$$\begin{aligned}
y_1' &= y_2,\\
y_2' &= \frac{1}{\alpha}\left(\beta J^2 e^{-2y_1} + y_4 - (y_6+\chi(y_8)) - y_3 e^{-y_1}\right),\\
y_3' &= -\frac{J}{\tau_p(y_4)} - y_2 e^{y_1}(y_6+\chi(y_8)),\\
y_4' &= \frac{e^{-y_1}}{\gamma}\left(\frac{5}{2}Jy_4 - \beta J^2 e^{-2y_1} + \frac{1}{2}J(y_6+\chi(y_8)) - y_5 - \frac{3}{2}J(y_4 - y_3 e^{-y_1})\right),\\
y_5' &= -\frac{1}{2\beta\tau_w(y_4)}\left(e^{y_1}(2y_4 - 3 + y_6 + \chi(y_8)) + y_3\right),\\
y_6' &= \frac{y_7}{\varepsilon(y_8)},\\
y_7' &= \sigma(N_D(y_8) - e^{y_1});
\end{aligned} \tag{3.39}$$

the boundary conditions read

$$\begin{aligned} &y_1(0) = y_1(1) = 0,\ y_2(0) = \ y_2(1) = 0, \\ &y_4(0) = y_4(1) = 1, \\ &y_6(0) = -V_{app},\ y_6(1) = 0. \end{aligned} \tag{3.40}$$

Equations (3.39) and (3.40) build our first-order system with boundary values depending on the parameter V_{app}. Such a problem can be easily solved with the code AUTO [8]; this software implements Keller's continuation method on the system discretized by collocation in finite element-like spaces. The method is known as very robust, even for strong nonlinearities; in particular, if the unknowns must be continuous, the use of finite element-like spaces allows to accomodate discontinuous derivatives.

3.2. *Numerical results*

Before presenting our results, it is worthwhile noticing that the first results for the steady-state QHD model showing a negative differential resistivity for the RTD have been obtained in[27], using a quasi-gradient method to minimize the energy functional together with a generalized Gummel algorithm and a P_1 finite element discretization. Later on, the same kind of results have been obtained as the long time solution of the transient QDD model[20], with the help of a decoupling preserving the positivity of the electronic density, as shown in[19].

For our computations, the physical quantities are defined as follows. The index $i = 1$ is used for a $GaAs$ layer and $i = 2$ for a Al$GaAs$ layer and there is no index for a quantity which is constant across all layers. The effective mass of the electrons is $m = m_r m_e$ (m_e the electron mass), the permittivities are given by $\varepsilon_i \varepsilon_0$ (ε_0 the vacuum permittivity), the doping profiles by N_{D_i}; the height of the potential barrier is denoted by H and the momentum relaxation time by τ_{p_0}. For the QHD model, we need also the thermal conductivity, modelled by $\kappa = \kappa_0 \frac{k_B^2 T_0}{m} n$. The relaxation times are either constants $\tau_p = \tau_{p_0}$, $\tau_w = \tau_{p_0}/a$ or given by the well-known model of ref.[2]:

$$\tau_p = \tau_{p_0} \frac{T_0}{T},\ \tau_w = \frac{\tau_p}{a}\left(1 + \frac{3k_B}{v_s^2}\frac{T^2}{T+T_0}\right), v_s = 2\times 10^5\ \mathrm{ms}^{-1}. \tag{3.41}$$

The geometry has been specified in Section 2.1; a first set of parameters for simulating the device of Ref.[21] are given in the Table 1.

m_r	ε_1	ε_2	$\mathrm{N}_{D_1}[cm^{-3}]$	$\mathrm{N}_{D_2}[cm^{-3}]$	H[eV]	$\tau_{p_0}[ps]$	κ_0
0.069	13.1	12.3	10^{18}	10^{15}	0.3	0.1	0.1

Table 1: First set of parameters

A first interesting question is to check that is the simplest model is able to produce a negative differential resistivity; therefore, we made simulations using the QDD model, with physical parameters summarized in Table 1. As can be seen on Figure 2, where the electric current in kA/cm^2 is plotted against the applied voltage in V, at low temperature the IV-curve shows a negative slope. Notice that all the IV curves below will be plotted using the same units, except in Fig. 5 where the current is given in a logarithmic scale.

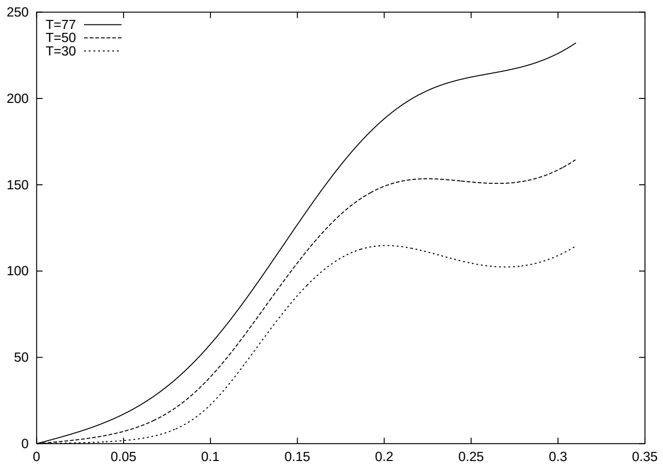

Figure 2: IV curves for the QDD model

In Figure 3, we compare, at room temperature $T_0 = 300°K$, the QDD model and the isothermal QHD model. Notice the curve for the QDD model looks like the one for the drift-diffusion model without quantum correction, whereas the convection term introduces a resonant behaviour. However, the magnitude of the current for the latter case seems to be quite wrong, compared to the other models; hence for these specific values of the parameters the convection has an effect, but it seems that for physical regimes, the negative differential resistivity is more likely due to the quantum corrections.

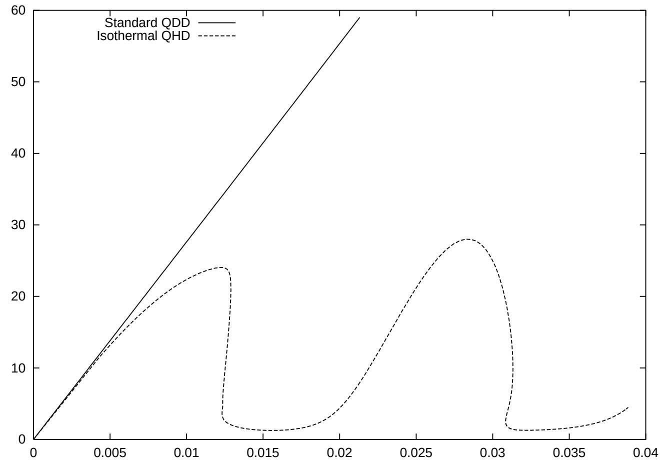

Figure 3: Standard QDD and isothermal QHD models

Next, we present in Figure 4, results obtained with the QHD model at $T_0 = 300°K$, either with the T-dependent ("Bac") or constant ("const") relaxation times models, the values of a are indicated on the figure. Notice that these different models for the relaxation times may change the quantitative results quite much.

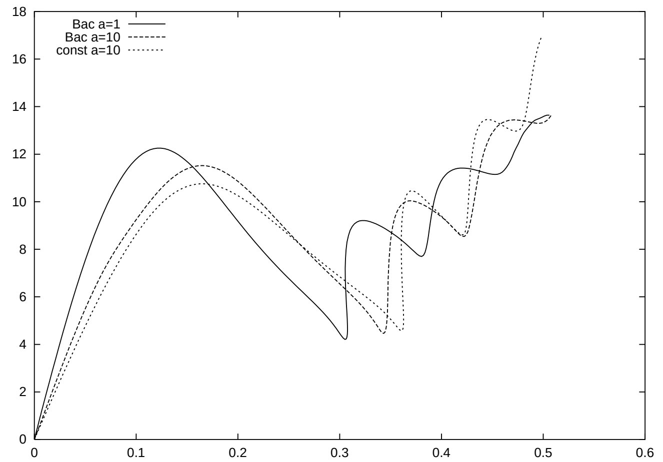

Figure 4: QHD model with different relaxation times

A comparison of the QDD model and the standard QHD model or a QHD model for which we have simply dropped the convection term in (2.10), in order to see its effect, is made in Figure 5; the current is in logarithmic scale convection, the relaxation times are constant and $a = 2$ and $T_0 = 300°K$. We do not observe a large difference between the two versions of the QHD model; on the other hand, the magnitude of the current obtained from the QDD model is much larger.

m_r	ε_1	ε_2	$N_{D_1}[cm^{-3}]$	$N_{D_2}[cm^{-3}]$	H[eV]	$\tau_{p_0}[ps]$	κ_0
0.063	12.9	12.0	10^{18}	5.010^{15}	0.3	0.1	0.8

Table 2: Second set of parameters

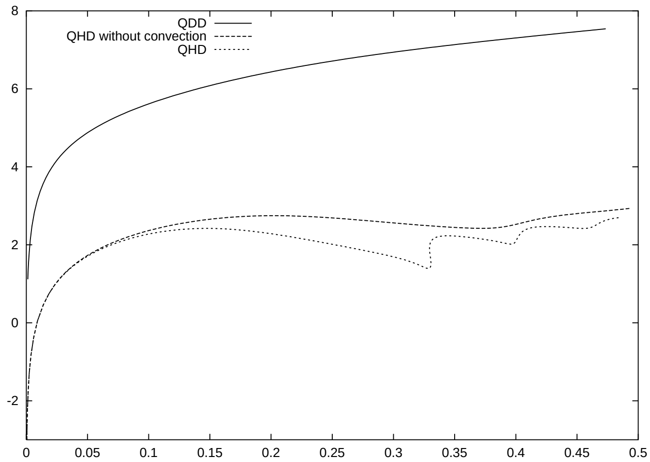

Figure 5: Comparison of QHD and QDD models

An interesting question is the one of hysteresis[12],[21] in the QHD model. First, we tried to obtain it by increasing the applied voltage and then decreasing it, which seems to be a standard way to proceed; we had no success.

Another idea related to this problem is to consider the hysteresis curve as a bifurcation diagram. With the help of the numerical bifurcation detection in AUTO, we did not get any bifurcation for the whole IV curve presented in Fig. 6 and also for the complete diagram obtained by adding to it the symmetric curve for which V is negative. Notice that the parameters for these computations are given in Table 2; the lattice temperature is $T_0 = 77°K$, the relaxation times are given by (3.41) with $a = 2$.

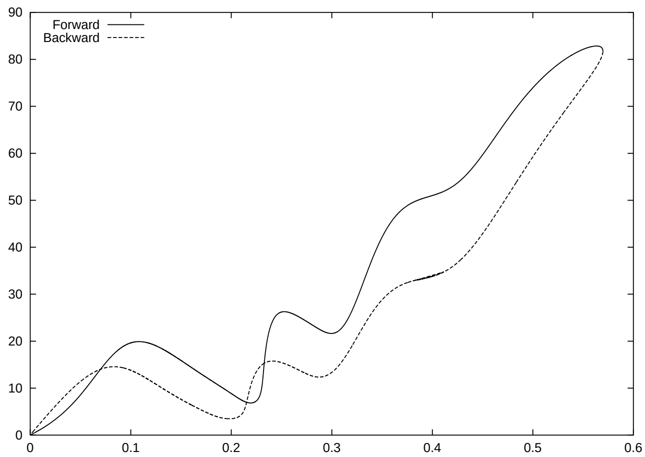

Figure 6: Complete IV-curve for QHD model

The behaviour of the curve in Fig. 6 (V reaches a maximum value, curve turns back and crosses itself at some points) suggested that the crossings are not true bifurcations. In order to see that there is no real intersection but that the solutions are not the same on each part of the curve, one has to find another parameter characterizing these solutions and to plot it on to a 3D diagram together with I and V. This was done with the software VBM[26].

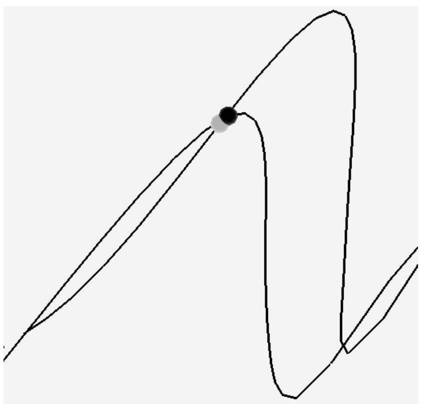

Figure 7: 2D view of bifurcation diagram

In Fig. 7, we plotted a region of the 2D IV curve containing the origin (first crossing at the left). There are two markers; the grey one is on the forward (increasing V) part, the black one on the backward part. The qualitative behaviour of the corresponding electronic density is shown respectively on Fig. 8a and Fig. 8b.

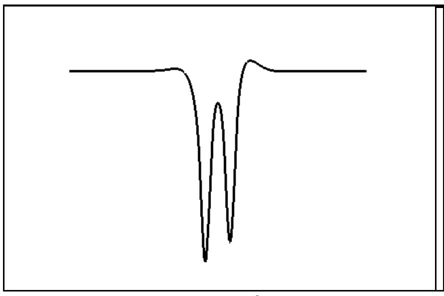

Figure 8a: Density for increasing voltage

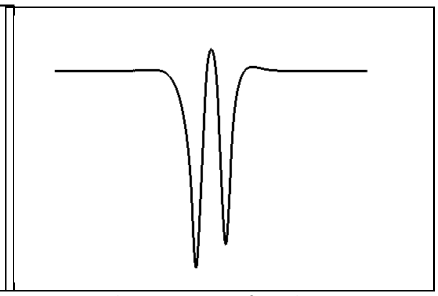

Figure 8b: Density for decreasing voltage

As suggested in[21], the electron distribution on the forward part of the curve is different from that on the backward part. In the first case, there is an accumulation of electrons just after the second barrier; in the second case, a part of these electrons have moved into the well, making the maximum of the density larger. The bifurcation diagram will then be obtained by plotting the current I, the applied voltage V and the third paremeter $nmax = \|ln(n)\|_\infty$ as a curve in $\Re^3$; a perspective projection of this curve on the plane is pictured on Fig. 9.

Figure 9: The complete bifurcation diagram

This diagram shows that there is no real crossing nor bifurcation; we see in particular that the markers which are on the same point on the 2D curve of Fig. 7 correspond to two different points on the 3D diagram.

4. Results for the smooth QDD model

4.1. *Numerical method*

The formal equations of our final model are obtained from (2.22-2.25) in the following way. First, we drop the convection term $(J^2/n)'$ in the momentum equation (2.24), which is certainly a good approximation at low current; then, the resulting equation yields an expression of the current J which is used in the mass conservation equation $J' = 0$. Finally, we obtain a second order elliptic system for the unknowns (ϕ, n), which we can write in each different layer:

$$-(\varepsilon\phi')' = \frac{q}{\varepsilon_0}(N_D - n), \tag{4.42}$$

$$k_B T_0 n'' + \frac{\hbar^2}{4mT_0}\left(n\overline{V}''\right)'' + nV'' = 0. \tag{4.43}$$

Of course, we have to provide interface and boundary conditions. The electrostatic potential ϕ and the current J given by (2.24) (without convection), have to be continuous across the layer interfaces; in fact, as we choose a standard Galerkin variational formulation of (4.42,4.43), the interface conditions are automatically taken into account. As far as the (essential) boundary conditions are concerned, we set

$$\phi(0) = -V_{app}, \phi(L) = 0;$$

if our computation domain is large enough, we can reasonably choose for the density:

$$n(0) = N_D(0),\ n(L) = N_D(L).$$

The approximate solution of the problem is obtained with a standard P_1 finite element dicretization of our weak variational formulation together with a Newton method to resolve the nonlinearity of the Poisson equation.

The smooth potential term $\overline{V}''$, given by the second derivative of the convolution (2.19) written in the discrete case, can be decomposed into two parts since $V = -(q\phi + \chi)$. The one part depending on the affinity is constant during the iterations and can be quite easily approximated because χ is made up of Heaviside functions; the other one is computed with an integration formula.

4.2. *Numerical results*

We wanted to know if the smooth QDD model formulated as a second order elliptic boundary value problem has the same behaviour as its analoguous hydrodynamic model. We made computations for the device of Ref.[14], with a lattice temperature equal to $300°K$; the relaxation times are chosen to be constant in each layer, given by the material mobility. The maximum height of the potential barrier that we were able to reach is $0.045\ eV$.

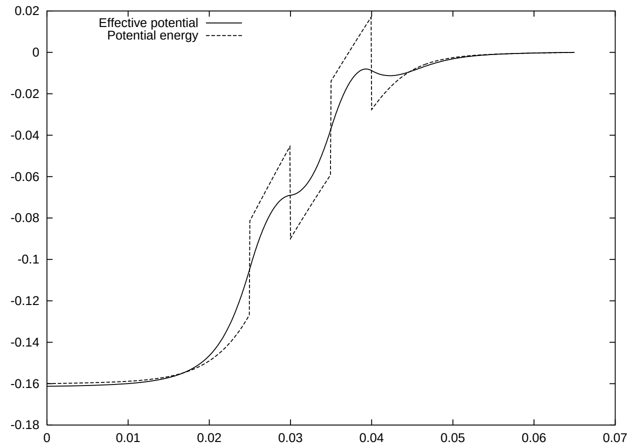

Figure 10: Potential energy and smoothed potential

First, we display in Fig. 10 the effective potential (eq. (2.19)) compared to the true discontinuous potential energy, for showing the smoothing effect. The corresponding IV-curve is pictured on Fig. 11, revealing the beginning of a negative slope region. Unfortunately, the computation could not go further, because the diffusion coefficient (i.e. the coefficient of n'' in eq. (4.43)) started to be negative; Fig. 12 depicts the situation just before it happens. We also noticed that, at this stage, the electronic density is very close to zero in the whole device. Continuing the computation leeds to the unphysical case of a negative density.

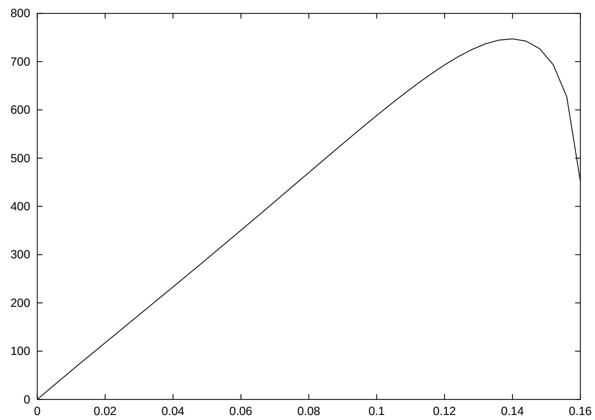

Figure 11: IV curve for smoothed potential

In order to prevent the occurence of a negative diffusion coefficient, one could use "the exponential form" of the smooth QDD model as suggested in [14], which consists in replacing the diagonal part of the stress tensor (2.20) by

$$P_{ii} = -nk_B T exp(\frac{\hbar^2}{4mk_B T^2}\frac{\partial^2 \overline{V}}{\partial x_i^2}); \tag{4.44}$$

the expansion of the exponential for a small argument coincides with (2.20) "to leading order in βV"[14]. Once again, we are not convinced that βV is very small for realistic devices (for example with a barrier height H=0.2eV and a temperature of 300°K: $\beta H \approx 7.7$ or $\beta q V_{app} \approx 98.7 V_{app}$ with V_{app} in Volts) and furthermore, at least to our knowledge, there is no derivation of this model and no explicit mention in the literature that it has been used in place of the smooth QHD or QDD model. One could also argue that the specific form (2.20) is due to the Born approximation; this will be discussed in more details in the next section.

Another conclusion of our simulations is that the larger the potential barrier is, the lower the value of the applied voltage at which this phenomenon appears. As a consequence, if the potential barrier is high enough (e.g. has the standard value corresponding to the physical properties of the different layers), the "diffusion" coefficient in eq. (4.43) appears to be negative (or more precisely to change its sign) even at zero applied voltage; this is the reason that makes computations impossible with this model if the barrier is realistic. In the next section, we give a theoretical argument for this behaviour.

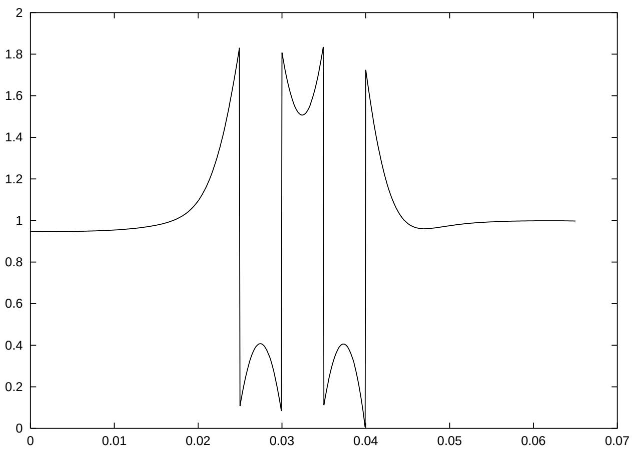

Figure 12: Diffusion coefficient at 0.16V

4.3. *An argument using the Bloch equation*

One can think that the negative "diffusion coefficient" in the equation (4.43) obtained by setting $J' = 0$ is due to the replacement of the true equilibrium Wigner distribution by it's Born approximation and that using the true equilibrium distribution will cure this problem. In fact, this is wrong as we shall see in this paragraph, by computing the current obtained with the true equilibrium distribution, or more exactly, from the solution of the Bloch equation (2.16).

Writing the one-dimensional version of this equation in the bounded domain $\Omega = (-A, L + A)$, $A > 0$ (we extend V by zero outside $[0, L]$) , yields

$$\frac{\partial \rho_e}{\partial \beta}(x, y;\beta) - \frac{\hbar^2}{2m}\rho_e''(x, y;\beta) + V(x)\rho_e(x, y;\beta) = 0 \ , \ x, y{\in}\Omega, \beta > 0, \qquad (4.45)$$

$$\rho_e(x, y;0) = \delta(x - y). \tag{4.46}$$

For physical reasons, for fixed β and y, the density matrix shall vanish for $|x|$ sufficiently large; hence, we can assume to compute the equilibrium density by solving the problem in Ω with homogeneous Dirichlet boundary conditions, provided we choose A large enough. Equation (4.45) is nothing else but the heat equation with β as the time and y a parameter.

The electrostatic potential beeing continuous, the potential energy $V = -(q\phi + \chi)$ is piecewise continuous (and hence bounded); we consider the following Sturm-Liouville problem

$$-\frac{\hbar^2}{2m}\psi''_\alpha(x) + V(x)\psi_\alpha(x) = E_\alpha\psi_\alpha(x),\ x \in \Omega, \tag{4.47}$$
$$\psi_\alpha(x) = 0,\ x \in \partial\Omega,\ \int_\Omega |\psi_\alpha|^2\, dx = 1.$$

Then the system $\{\psi_\alpha\}_\alpha$ builds a Hilbert basis of $L^2(\Omega)$, a basis of $H^1_0(\Omega)$ and the eigenvalues are distinct and can be ordered: $E_1 < E_2 < ..E_k < E_{k+1} < ....$ Using this basis, we get

$$\rho_e(x, y;\beta) = \sum_\alpha c_\alpha(y, \beta)\psi_\alpha(x),\ c_\alpha(y, \beta) = \int_\Omega \psi_\alpha(x)\rho_e(x, y;\beta)\ dx,$$

and inserting this representation in (4.45), we obtain after a straightforward computation:

$$c_\alpha(y, \beta) = e^{-\beta E_\alpha}c_\alpha(y, 0) = e^{-\beta E_\alpha}\psi_\alpha(y).$$

Finally, we can deduce the following formula, which is usually assumed in the case of a bounded domain, for the density matrix:

$$\rho_e(x, y;\beta) = \sum_\alpha e^{-\beta E_\alpha}\psi_\alpha(x)\psi_\alpha(y),\ x, y{\in}\Omega, \beta > 0. \tag{4.48}$$

If we use (2.15), (2.18) and recall that

$$< \frac{p^2}{m} > \ = mnu^2 - P,$$

we can compute the stress-tensor by

$$P(x) = \frac{n(x)}{\widetilde{\rho}_e(x, 0; \beta)}\frac{\hbar^2}{m}\frac{\partial^2\widetilde{\rho}_e}{\partial s^2}(x, 0; \beta).$$

It is straightforward to show, with the help of (2.18), (4.48) and (4.47) that

$$P(x) = (nV)(x) - \frac{n(x)}{n_{eq}(x)} \sum_{\alpha} e^{-\beta E_\alpha} \left(E_\alpha \psi_\alpha(x)^2 + \frac{\hbar^2}{2m} \psi'_\alpha(x)^2 \right),$$

where we set (dropping the dependence on β) :

$$n_{eq}(x) = \rho_e(x, x; \beta). \tag{4.49}$$

A tedious but easy computation allows us to obtain for the smooth quantum drift-diffusion model:

$$J(x) = \frac{m}{\tau_p} \left(P' - nV' \right)(x) = -D(x) \left(n'(x) - \frac{n'_{eq}(x)}{n_{eq}(x)} \right). \tag{4.50}$$

with

$$D(x) = \frac{1}{n_{eq}(x)} \sum_{\alpha} e^{-\beta E_\alpha} \left(E_\alpha \psi_\alpha(x)^2 + \frac{\hbar^2}{2m} \psi'_\alpha(x)^2 \right) - V(x).$$

The last equation defines the diffusion coefficient of the elliptic problem obtained by using $J' = 0$ and (4.50). At the interfaces between the different layers, the quantities ψ_α, ψ'_α and n_{eq} are continuous. Hence, the jump of D is given by

$$\{D\} = \{\chi\}, \tag{4.51}$$

which means that when entering from the left into a potential barrier, the diffusion coefficient decreases quite much for large affinity.

In the case $V = 0$, we can solve the eigenvalue problem to get:

$$\psi_\alpha(x) = \sqrt{\frac{2}{b}} sin \left(\sqrt{\frac{2mE_\alpha}{\hbar^2}} (x + A) \right), \; E_\alpha = \frac{\pi^2 \hbar^2}{2mb^2} \alpha^2, \; \alpha = 1, 2, 3, ..., \; b = L + 2A, \tag{4.52}$$

while the solution of the Bloch equation is given by

$$\rho_e(x, y;\beta) = \frac{1}{2\sqrt{\pi}\lambda_D} e^{- \; \frac{x-y}{2\lambda_D} \;^2}, \; \lambda_D = \sqrt{\frac{\hbar^2 \beta}{2m}}. \tag{4.53}$$

Then, using (4.52), (4.49), (4.53) and

$$\sum_{\alpha=1}^{\infty} e^{-\beta E_\alpha} E_\alpha = -\frac{d}{d\beta} \sum_{\alpha=1}^{\infty} e^{-\beta E_\alpha} \doteqdot -\frac{d}{d\beta} \left(\int_0^\infty e^{-\frac{\beta \pi^2 \hbar^2}{2mb^2} \alpha^2} d\alpha \right) = \frac{b}{4\beta\sqrt{\pi}} \frac{1}{\lambda_D},$$

we can approximate the diffusion coefficient as follows:

$$D(x) = 2\sqrt{\pi}\lambda_D \sum_{\alpha=1}^{\infty} e^{-\beta E_\alpha} \left(\frac{2}{b} E_\alpha\right) \doteqdot \frac{1}{\beta}. \tag{4.54}$$

Approximating the potential by $V_0 - \chi$ for the equilibrium state (no applied voltage) and denoting by $(L-\delta)/2$ (resp. by $(L+\delta)/2$) the location of the right boundary of the first barrier (resp. of the left boundary of the second barrier), we notice that for δ/A small, the non vanishing V_0 does not affect too much the solution of the eigenproblem (4.47) outside $((L-\delta)/2, (L+\delta)/2)$. Hence, we can estimate the jump at $x = (L-\delta)/2$ by

$$\{D\} \doteqdot \frac{1}{\beta} - H; \tag{4.55}$$

at room temperature, one has $1/\beta = 0.026\ eV$, and the diffusion coefficient becomes certainly negative for physical values of H in the range $0.2 - 0.3\ eV$.

5. Results for the Schroedinger-Poisson model

5.1. *Numerical methods*

In order to compute the current by eq. (2.29), we need to know the values of the Fermi energies, the electrostatic potential and the solutions of the Schroedinger problems (2.26-2.28) for computing the transmission coefficient at points required by a quadrature rule for the integral.

For the Fermi energy μ_0, by using the Fermi distribution and a change of variable, we get

$$N_D(0) = N_C \mathcal{F}_{1/2}\left(\frac{\mu_0 - V_0}{kT_0}\right), \; N_C = \frac{1}{4}\left(\frac{2mkT_0}{\pi\hbar^2}\right)^{3/2},$$

and we approximate the inverse function $\mathcal{N}_{1/2}$ of the Fermi integral $\mathcal{F}_{1/2}$ in the following way[6]

$$\mathcal{N}_{1/2}(u) \approx f(u) = \frac{\ln u}{1-u^2} + \frac{\left(\frac{3}{4}\sqrt{\pi}u\right)^{2/3}}{1 + \left(0.24 + 1.08\left(\frac{3}{4}\sqrt{\pi}u\right)^{2/3}\right)^{-2}},$$

to get

$$\mu_0 = V_0 + kT_0 F(N_D(0)/N_C).$$

For the LSP linear model, the electrostatic potential is given by either a piecewise P_1 or a piecewise P_2 polynomial. In the first case, the potential passes from V_0 to V_L in a region containing the device plus a small interval before the first and after the second barrier by respecting the continuity of ϕ and $\varepsilon\phi'$; in the second case, the potential is obtained by solving Poisson equation, with $n = 0.15 * N_D(0)$ in the device and $n = N_D(0)$ outside.

For a given value of k (or E), approximate solutions of problems (2.26-2.28) are computed by a standard P_1 finite elements discretization and using Lapack to solve the resulting linear systems with tridiagonal matrices.

After a change of variable, the integral for the current can be split in two parts

$$J = \frac{qm(kT_0)^2}{2\pi^2\hbar^3}\left[\int_0^{y_0} f_1(y)dy + \int_0^{\infty} \exp(-y) f_2(y)dy\right],$$

with

$$f_1(y) = \ln\left(\frac{1+\exp\left(\frac{\mu_0 - V_0}{kT_0} - y\right)}{1+\exp\left(\frac{\mu_L - V_0}{kT_0} - y\right)}\right) T(V_0 + kT_0 y), \;\; f_2(y) = exp(y - y_0) f_1(y + y_0).$$

The first integral is computed with a Gauss-Legendre rule, adjusting y_0 to garantee enough accuracy, the second one is performed with a Gauss-Laguerre rule. A similar process is applied to the integral for the density for the real nonlinear model, where we have to compute from (2.31) the electronic density appearing in the r.h.s. of Poisson equation (2.8).

5.2. *Numerical results*

We have computed the solutions of the **LSP** model (i.e. the linear model with given electrostatic potential) for the two forms of given elecrostatic potential described above. The device is essentially the one of reference[21] and the physical parameters can be read from Table 2, except the potential barrier which is $H = 0.209$ eV. The lattice temperature, which appears as a constant in the model is equal to $300°K$.

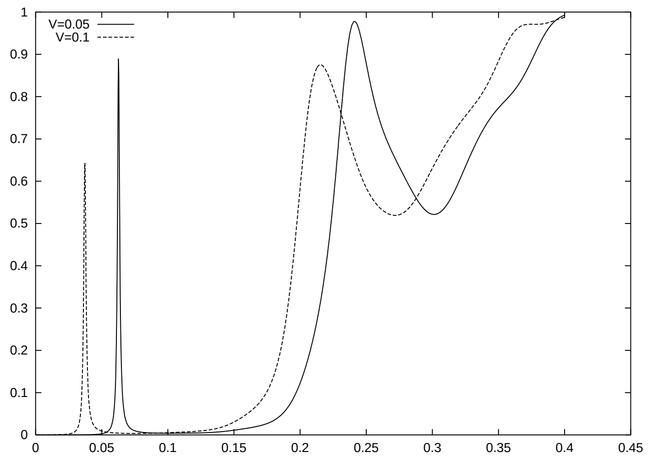

Figure 13: Transmission coefficient T(E)

The resonance effect appears clearly on Fig. 13, where the graph of the transmission coefficient (2.30) is plotted in function of the energy in eV. Notice that the effect is more pronounced for low applied voltage. The IV-curves for the two given potential are plotted on Fig. 14. They have a good qualitative behaviour but indicate that the value of the current depends effectively on the electrostatic potential. If we compare these curves with those of the QHD model (Fig. 4), one observes that the position of the first maximum is about the same, but the current value at this point is much larger in the LSP model.

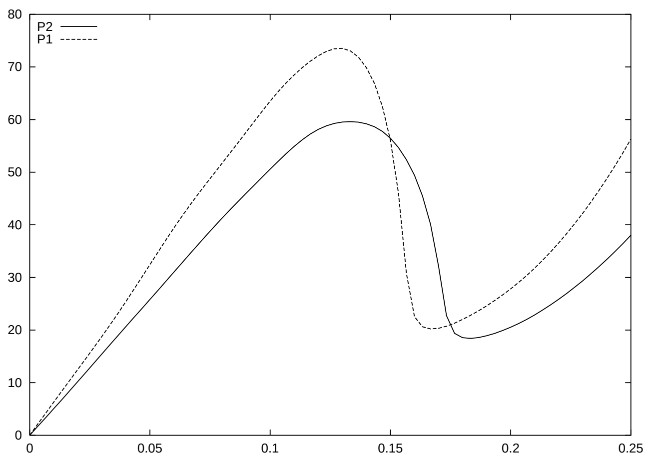

Figure 14: IV-curve for 2 given potentials

For the true nonlinear SP model, the nonlinearity of the Poisson equation has been resolved using fixed-point like iterations, but on the equation with an extra artificial discrete time derivative term that stabilizes the successive linear systems. In fact, for a regular mesh, it is an underelaxation method. This algorithm requires a very fine mesh to converge, is slow and the results may depend on the size of the domain. For this reason, a more efficient pseudo-Newton method will be set up and other numerical results published in a forthcoming paper. Nevertheless, we present in Figure 15, the IV-curve for the device described at the beginning of this section but for two different temperatures. Obviously, the current is larger than the one obtained from the other models, the first maximum is displaced to the right and is higher. Compared to the picture of Reference[23] (p. 24), we notice that the position and height of the first maximum is roughly the same, but the shape of the curves is very different. Furthermore, the behaviour of the current from zero until the maximum and the maximum height are not quite the same for the two temperatures.

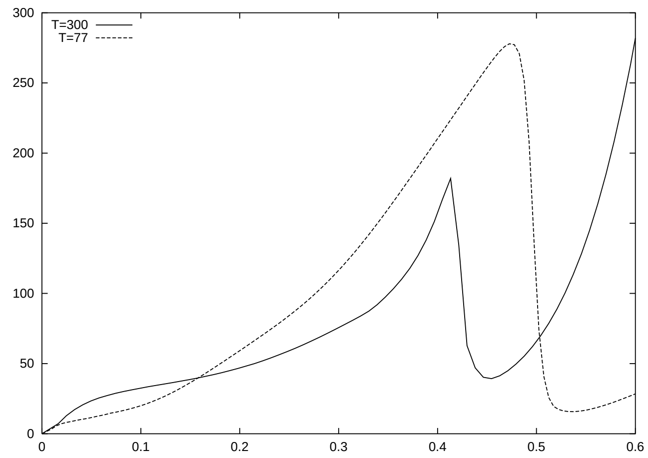

Figure 15: IV-curve for the SP model

6. Conclusion

In this paper, we have presented three basic models (with several variations) for simulating quantum effects in semiconductors and we have computed numerical results. All the models we were able to simulate can reproduce, at least qualitatively and for ad hoc chosen values of the parameters, the negative differential resistivity characteristic of the test device.

For the standard quantum hydrodynamic and quantum drift-diffusion models, we have noticed that, as in the models without quantum corrections, the results are quite sensitive to the physical parameters (such as the model for the mobility or the thermal conductivity). Hence, before getting significant results for simulating a specific device, all the parameters have to be adjusted by some fitting of the IV curves with some experimental results or results of simulation using other models.

Consequently, one can believe that the model which has the smaller number of parameters, namely the Schrödinger-Poisson model, would be the better and the easier to use. For the linear (LSP) model, where the electrostatic potential has a given shape, the solution can be computed at a low CPU time price. But, for the real nonlinear problem, where we have to solve the Poisson equation with the electronic density depending on the potential, the use of a fixed-point like method has shown slow convergence and also a prohibitive CPU time, because one has to use a very fine mesh. Furthermore, the magnitude of the current for the pure quantum Schrödinger-Poisson model, although of the same order, is not the same as the one of the hydrodynamic or drift-diffusion models with quantum corrections and furthermore the shape of the IV-curves is quite different. This is not so surprising because of the very different nature of the models, the SP model being unable to account for relaxation-like collisional effects.

Hence, we believe that the standard hydrodynamic model with quantum corrections is able, after the parameters have been well fitted, to reproduce a larger amount of physical effects at a quite low cost, at least in one or two space dimensions.

References

1. A. Arnold, *On absorbing boundary conditions for quantum transport equations, M2AN* **28** (1994) 853-872.
2. G. Baccarani and M.R. Wordeman, *An Investigation of Steady-State Velocity Overshoot in Silicon, Solid-State Electronics* **28** (1985) 407-416.
3. N. Ben Abdallah, *On a Multi-Dimensional Schrödinger-Poisson Scattering Model for Semiconductors*, *Z. angew. Math. Phys.* **48** (1997) 135-155.
4. N. Ben Abdallah and A. Unterreiter, *On the Stationary Quantum Drift-Diffusion Model, Z. angew. Math. Phys.* **49** (1998) 251-275.
5. N. Ben Abdallah P. Degond and P.A. Markowich, *On a one-dimensional Schrödinger-Poisson Scattering model, Z. angew. Math. Phys.* **48** (1997) 35-55.
6. J. S. Blakemore, *Approximation for Fermi-Dirac Integrals, Especially the Function $\mathcal{F}_{1/2}(\eta)$ Used to Describe Electron Density in a Semiconductor, Solid-State Electronics* **25** (1982) 1067-1076.
7. Ph. Caussignac, B. Zimmermann and R. Ferro, *Finite Element Approximation of Electrostatic Potential in One Dimesional Multilyaer Structures with Quantized Electronic Charge*, *Computing* **45** (1990) 251-264.
8. E. Doedel, H.B. Keller and J.P. Kernevez, *Numerical analysis and control of bifurcation problems (II) Bifurcation in inifinite dimensions, Int. J. Bifurcation Chaos* **1** (1991) 745-772.
9. D.K. Ferry and Jing-Rong Zhou, *Form of the quantum potential for use in hydrodynamic equations for semiconductor device modeling*, *Phys. Rev.* **B48** (1993) 7944-7950.
10. W. R. Frensley, *Simulation of resonant-tunneling heterostructure devices, Journal of Vacuum Science and Technology* **B3** (1985) 1261-1266.
11. W. R. Frensley, *Boundary Conditions for open Quantum Systems driven far from Equilibrium, Reviews of Modern Physics* **62** (1990) 745-791.
12. C.L. Gardner, *The Quantum Hydrodynamic Model for Semiconductor Devices*, *SIAM J. Appl. Math.* **54** (1994) 409-427.
13. C.L. Gardner and C. Ringhofer, *The Smooth Quantum Potential for the Hydrodynamic Model*, *Phys. Rev.* **E53** (1996) 157-167.
14. C.L. Gardner and C. Ringhofer, *Numerical Simulation of the Smooth Quantum Hydrodynamic Model for Semiconductor Devices, Comp. Meth. Appl. Eng.* **181** (2000) 393-401.
15. I. Gasser, P.A. Markowich and C. Ringhofer, *Closure Conditions for Classical and Quantum Moment Hierarchies in the Small Temperature Limit, Transport Theory and Statistical Physics* **25** (1996) 409-423.
16. I. Gasser, P.A. Markowich, D. Schmidt and A. Unterreiter, *Macroscopic Theory of Charged Quantum fluids,* in Mathematical problems in semiconductor physics, Marcati, P. et al. (ed.), Harlow: Longman, Pitman Res. Notes Math. Ser. 340, 42-75 (*1995).*
17. H.L. Grubin, T.R. Govindan, J.P. Kreskovsky and M.A. Stroscio, *Transport via the Liouville Equation and Moments of Quantum Distribution Functions*, *Solid-State Electronics* **36** (1993) 1697-1709.
18. B. Jogai, C.I. Huang and C.A. Bozada, *Electron density in quantum well diodes J. Appl. Phys.* **66** (1989) 3126-3130.
19. A. Juengel and R. Pinnau, *Global non-negative solutions of a nonlinear fourth-*

order parabolic equation for quantum systems, SIAM J. Math. Anal. **32** (2000) 760-777.
20. A. Juengel and R. Pinnau, *A positivity preserving numerical scheme for a nonlinear fourth-order parabolic system, SIAM J. Numer. Anal.* **39** (2001) 385-406.
21. N.C. Kluksdahl, A.M. Kriman, D.K. Ferry and C. Ringhofer, *Self-consistent study of the resonant-tunnelling diode, Phys. Rev.* **B39** (1989) 7720-7735.
22. A. Messiah, **Quantum Mechanics**, Vol. 1, (North-Holland, 1970), Chap.VI.
23. H. Mizuta and T. Tanoue, ***The Physics and Applications of Resonant Tunnelling Diodes (*** Cambridge University Press, 1995).
24. F. Nier, *A stationary Schrödinger-Poisson system arising from the modelling of electronic devices*, *Forum-Math.* **2** (1990) 489-510.
25. F. Nier, *A variational formulation of Schrödinger-Poisson systems in dimension 3, Comm. Part. Diff. Equations* **18** (1993) 1125-1147.
26. R.C. Paffenroth, *Mathematical Visualization, Parameter Continuation and Steered Computations*, PhD Thesis, University of Maryland (1999) and URL: *http://lcvmwww.epfl.ch/VBM.*
27. R. Pinnau and A. Unterreiter, *The Stationnary Current-Voltage Characteristics of the Quantum Drift-Diffusion Model, SIAM J. Numer. Anal.* **37** (1999) 211-245.
28. H. Steinrueck and F. Odeh, *The Wigner function for thermal equilibrium*, *Journal of Appl. Math. Phys. (ZAMP)* **42** (1991) 471-487.
29. A. Unterreiter, *The Quantum Zero Space Charge Model for Semiconductors, Europ. J. Appl. Math.* **10** (1999) 395-415.
30. A. Wettstein, *Quantum Effects in MOS Devices,* PhD Thesis, ETH-Zürich (2000).
31. E.P. Wigner, *On the Quantum correction for Thermodynamic Equilibrium, Phys. Rev.* **40** (1932) 749-759.